Journal of Molecular Catalysis A: Chemical 313 (2009) 44–48

Contents lists available at ScienceDirect

Journal of Molecular Catalysis A: Chemical

journal homepage: www.elsevier.com/locate/molcata

Hydrothermal synthesis and characterization of phosphorous-doped TiO_2 with high photocatalytic activity for methylene blue degradation

C. Jin, R.Y. Zheng, Y. Guo, J.L. Xie, Y.X. Zhu*, Y.C. Xie

Beijing National Laboratory for Molecular Science, State Key Laboratory for Structural Chemistry of Unstable and Stable Species, College of Chemistry and Molecular Engineering, Peking University, 100871 Beijing, China

ARTICLE INFO

Article history:
Received 21 April 2009
Received in revised form 30 July 2009
Accepted 30 July 2009
Available online 8 August 2009

Keywords:
P-doped
Titania
Hydrothermal
Photocatalytic

ABSTRACT

Phosphorous-doped titania was synthesized by a one step hydrothermal method. These samples exist in anatase phase with much higher crystallinity compared to those prepared by conventional calcination method. In addition, P-doping induced additional hydroxyl groups on surfaces and decreased the numbers of oxygen vacancies in the bulk. Therefore, the methylene blue (MB) degradation performance on the phosphorous-doped photocatalyst is much enhanced and superior to that of the commercial P25. The hydrothermal method proves to be very suitable for the synthesis of P-doped titania photocatalyst.

1. Introduction

Heterogeneous photocatalysis by semiconductors has gained intense research interest in the past decades due to its applications in environmental purification and solar energy conversion [1,2]. It especially provides an economical and ecological method for the remediation of contaminated water and air [3,4]. Among various semiconductor oxides, TiO_2 proves to be the most suitable material because of its many desirable properties, such as strong oxidizing power, high photo- and thermal-stability, low price, facile synthesis and the low toxicity of titanium. However, the photocatalytic efficiency of pure TiO_2 needs to be improved to meet industrial requirements. Several methods have been devoted to enhance the photoactivity, among which, non-metal doping has attracted much attention recently. Many authors have reported the non-metal anion doped TiO_2 by N, B, C, S, F, Cl, and Br [5–15]. On the other hand, phosphorous-doped TiO_2, in which the non-metal element exists as a cation, may possess different surface and bulk properties and has aroused researchers' interest [16–23]. Yu et al. synthesized mesoporous phosphated TiO_2 with a wormlike structure by a P123 templating method [16]. Their results showed that the photo-oxidation rate of n-pentane was higher in the phosphated photocatalyst. Korosi et al. investigated the phosphate-modified TiO_2 synthesized by a sol–gel method [20]. Phosphate not only alters the surface property, but also affects the crystallization behavior and phase transformation of TiO_2. Our previous work also indicates that P-doped titania synthesized by a modified sol–gel method is effective for the degradation of 4-chlorophenol and methylene blue [19,23]. The doped phosphorus existed in a pentavalent oxidation state, replacing part of Ti^{4+} in the anatase lattice in the form of Ti–O–P bonds.

Hydrothermal treatment is widely applied to obtain metal oxide nanoparticles [24]. This wet chemical approach involves the crystallization of metal oxide at relatively low temperature and under autogenous pressure. By avoiding high-temperature calcinations, hydrothermal synthesis provides a simple route for preparing fine particles with well-crystallinity. According to literature, it is a common problem that P-doping or phosphate modification can retard the growth of titania [20,23], thus requiring a high calcination temperature to achieve well-crystallinity. This would definitely reduce the surface area and hydroxyl groups. To avoid these undesirable outcomes, hydrothermal method seems to be a suitable choice.

In the present work, hydrothermal method was chosen as a simple and effective way for the synthesis of P-doped TiO_2 with high crystallinity. The obtained products have more excellent photocatalytic activity under UV light for the degradation of methyl blue than the samples obtained by calcination. The effects of P-doping on surface and optical properties were also discussed.

2. Experimental

2.1. Catalyst preparation

For preparing phosphorous-doped TiO_2, 10.2 g tetrabutyl titanate was dissolved in 50 mL ethanol, and then this solution was

* Corresponding author. Tel.: +86 10 62751703.
E-mail address: zhuyx@pku.edu.cn (Y.X. Zhu).

1381-1169/$ – see front matter © 2009 Elsevier B.V. All rights reserved.
doi:10.1016/j.molcata.2009.07.021

added dropwise to 20 mL hypophosphorous acid solution under vigorous stirring. The P/TiO_2 molar ratio in the resulting suspension was 0.01, 0.02, 0.04 and 0.08, respectively. After being stirred for 2 h, the mixture was transferred to a 100 mL Teflon-lined stainless steel autoclave, followed by a hydrothermal treatment at 260 °C for 24 h. After the reaction, the powder sample was filtered, rinsed with ethanol and de-ionized water, and dried in oven at 110 °C for 12 h. The samples were denoted as HT001, HT002, HT004 and HT008. Pure TiO_2 without phosphorous doping was prepared by the same procedure except that tetrabutyl titanate was hydrolyzed in pure water.

High-temperature calcinated P-doped samples were also prepared in a similar way to the above except that the precipitates were rinsed, dried and calcined at 500 or 600 °C for 4 h. The obtained products with a 0.02 P/TiO_2 nominal molar ratio are denoted as CT002-500 and CT002-600, respectively.

2.2. Characterization techniques

The XRD patterns were acquired on a Rigaku D/MAX-200 diffractometer with Ni-filtered Cu Kα radiation at 40 kV and 100 mA. Surface area was measured by a Micromeritics ASAP 2010. Surface composition of the samples was analyzed on a Kratos Axis Ultra System with monochromatic Al Kα X-rays (1486.6 eV). Thermogravimetric analysis (TGA) experiments were carried out using a Q600SDT apparatus (Thermal Analysis Co. Ltd.) in a N_2 flow of 100 mL min^{-1}. The UV–vis spectra of the powder samples were recorded on a Shimadzu UV 3100 PC. TEM images were obtained on a FEI Tecnai F30 transmission electron microscope.

2.3. Photocatalytic activity test

The photocatalytic activities were evaluated by methylene blue (MB, $C_{16}H_{18}N_3S$) decomposition under UV and visible light irradiation. UV illumination was provided by a 6 W medium-pressure mercury lamp with a main emission peak at 254 nm. The visible light source was a 150 W halogen–tungsten lamp (Philips) equipped with a UV cut-off filter to remove the UV portion of the illumination (<400 nm). Catalyst powder (50.0 mg) was dispersed in 200 mL aqueous methylene blue (1.2×10^{-5} mol L^{-1}). The photocatalytic activity of catalysts was tested after magnetically stirring the suspension for 1 h in darkness to achieve adsorption–desorption equilibrium. At given time intervals, 4 mL suspension was taken and immediately centrifuged, and the light absorption of the clear solution was measured at 665 nm (λ_{max} for MB) by a UV–vis spectroscopy.

3. Results and discussion

3.1. Characterization of photocatalyst

3.1.1. XRD analysis

XRD patterns of pure titania and P-doped titania are displayed in Fig. 1(a). All the samples exhibits pure anatase diffraction pattern. Upon increasing phosphorous doping concentration, the peak intensity of anatase gradually decreases and the half-width of the diffraction peak is broadened. Average crystalline sizes calculated from the broadening of the (1 0 1) peak are listed in Table 1. The particle size becomes smaller as phosphorous concentration is increased, which is further proved by the TEM images (see supplementary content Fig. S1).

From Fig. 1(b), we can see that the diffraction peak intensity of CT002-600 is slightly stronger than that of CT002-500. However, when synthesized by a hydrothermal treatment at 260 °C, an extraordinary increase of peak intensity is observed, illustrating that the hydrothermal sample has higher crystallization

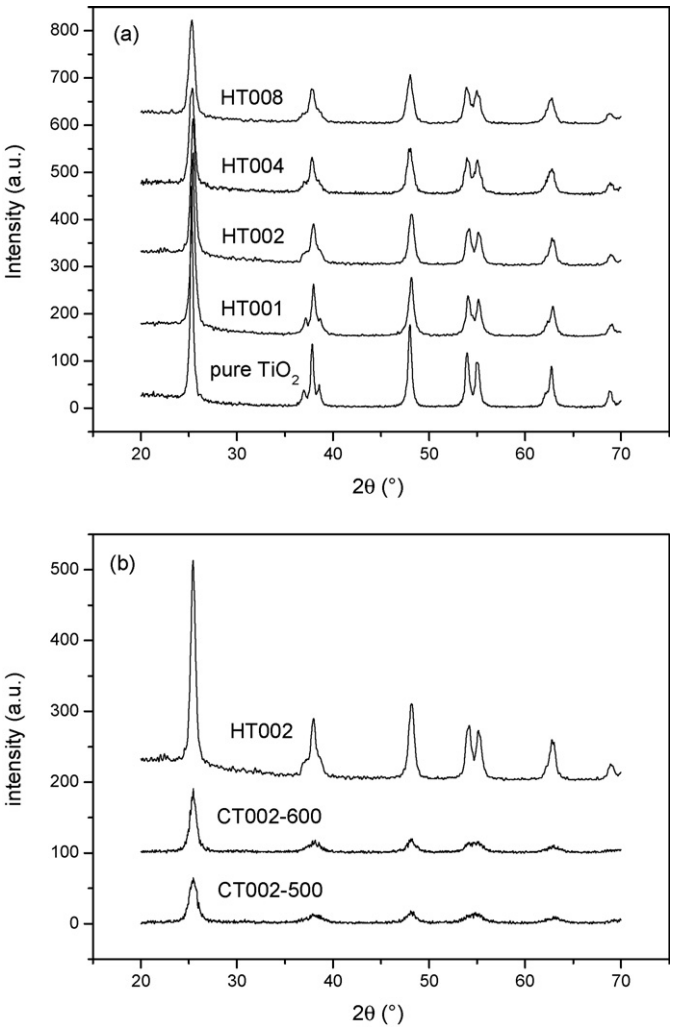

Fig. 1. (a) XRD pattern of hydrothermal synthesized titania with various phosphorous concentration; (b) XRD pattern of CT002-500, CT002-600 and HT002.

degree. To get a quantitative view of the crystallization degree, the area of (1 0 1) diffraction peak was integrated and the data is presented in Table 1. $I_{(101)}$ becomes smaller as phosphorous concentration increased. $I_{(101)}$ of HT008 drops to 75% of pure titania. The hydrothermal series has much higher crystallization degree than the calcined samples. $I_{(101)}$ of HT002 is nearly three times that of CT002-600. This could be ascribed to the repeated dissolution–precipitation process during the long hydrothermal period and it would generate highly crystallized nanoparticles. Many studies have pointed out that crystallization degree is an important factor which affects photocatalytic efficiency [11,25].

Table 1
Physi-chemical properties of pure and phosphorous-doped titania.

Sample	d_{XRD} (nm)[a]	$I_{(101)}$[b]	S_{BET} (m^2/g)	S_{cal} (m^2/g)	Average pore diameter (nm)
Pure titania	19.3	217	59	81	19.8
HT001	16.0	219	82	98	16.6
HT002	14.5	203	104	108	14.7
HT004	12.3	173	127	127	12.8
HT008	11.5	162	134	136	10.2
CT002-500	11.1	82	122	141	5.6
CT002-600	11.3	86	82	139	8.0

[a] Average diameter is calculated by the broadening of (1 0 1) diffraction peak.
[b] $I_{(101)}$ is the integrating intensity of (1 0 1) diffraction peak.

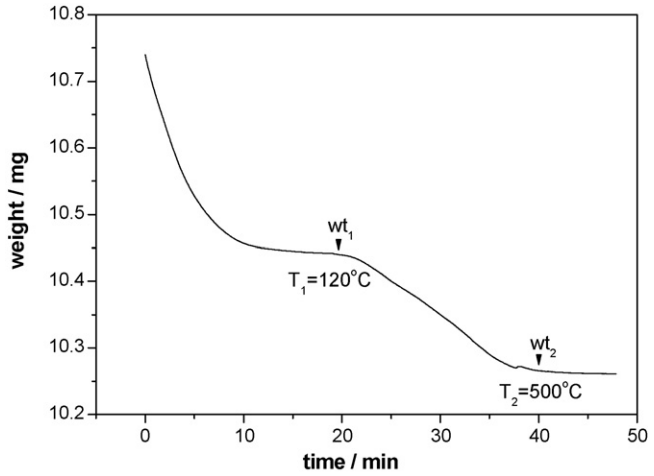

Fig. 2. Sample weight of HT002 as a function of TGA heating time. The OH surface density is based on the weight loss between 120 and 500 °C.

The promoted crystallization of titania nanoparticles by hydrothermal treatment would reduce defect sites on surface and enhance the photocatalytic activity.

3.1.2. Nitrogen adsorption analysis

From Table 1, it can be seen that S_{BET} of HT002 is twice that of pure sample. Phosphorous species inhibit the crystalline growth, thus remarkably enlarging the surface area. This phenomenon was also reported by other authors who used different phosphor-containing compound as precursor [18,21].

The particle size of HT002 is larger than CT002-500, but its surface area is higher than the latter, and comparable to that of CT002-600. Assuming the particles are spherical and unagglomerate, the theoretical surface area (S_{cal}) can be calculated by the equation: S_{cal} (m^2/g) = 1566/d, where d is the particle diameter determined from XRD. The results are presented in Table 1. The S_{BET} and S_{cal} of CT002-600 are 82 and 139 m^2/g, respectively, but these values for HT002 are 104 and 108 m^2/g. Huge discrepancies between S_{BET} and S_{cal} are observed for the calcined samples, while there is little difference for the samples obtained by hydrothermal method. Calcinations cause particles to form hard agglomerates while the hydrothermal treatment creates a softer agglomeration of particles [26], permitting substrate molecules to diffuse easily in the mesopores. In acquiring well-crystallinity, the hydrothermally treated samples still maintain high surface area.

3.1.3. Thermogravimetric analysis

TGA was used as a convenient method to determine the content of surface hydroxyl groups [27]. The titania powders were heated from 25 °C to T_1 = 120 °C at 10 °C/min, held at this temperature for 10 min to remove the physically absorbed water (step 1), and then heated at 20 °C/min to T_2 = 500 °C (step 2) in nitrogen. Step 2 represents the weight loss by the removal of hydroxyl groups from the powder surface (see Fig. 2). The OH surface density can be calculated by the following equation:

$$\#OH/nm^2 = \alpha \times \frac{(\#OH/nm^2)_{T_2} \times SSA \times wt_{T_2} + [(wt_{T_1} - wt_{T_2})/(MW_{H_2O}/N_A) \times 2]}{SSA \times wt_{T_1}} \quad (1)$$

Here, wt_{T_i} is the sample weight at the corresponding temperature T_i, SSA is the specific surface area, MW_{H_2O} is the molecular weight of water, N_A is Avogadro's constant, and R is a calibration factor. As can be seen in Table 2, the number of hydroxyl groups per unit area is lowered regularly with increased phosphorous content. After converting these values into the unit of OH per gram, it was found that OH density on all P-doped samples are nearly the same and higher than that on the pure titania to some extent. As an effect of P-doping, additional hydroxyl groups were added on the surfaces of titania.

Table 2
OH surface density on pure titania and P-doped samples.

Sample	OH (nm^2)	10^{-20} OH (g)
Pure TiO_2	9.9	5.8
TP002	6.2	7.2
TP004	5.7	7.2
TP008	5.0	6.7

3.1.4. XPS analysis

The chemical forms and concentrations of surface elements in the P-doped samples were investigated by XPS analysis. As shown in Fig. S2(a), the XPS peaks in the Ti 2p region appear at 458.6 (Ti 2p3/2) and 464.3 (Ti 2p1/2) eV for HT002. The binding energy of Ti 2p3/2 shifted to a positive value by 0.2 eV, when compared to that of undoped TiO_2 (458.4 eV, figure not shown). Further increasing the P/Ti ratio to 0.08 as it is in HT008, this peak moved to 458.9 eV. The more electronegative P^{5+} atom replaces the Ti^{4+} atom in the surface or near surface region, pulling the electrons in Ti–O bond a bit away form Ti atom, thus causing a little rise of Ti 2p3/2 binding energy. The state of P species is different from that of PO_4^{3-}. If pure titania was impregnated with Na_3PO_4, there is a peak in the IR spectrum between 1300 and 1400 cm^{-1}, which is the characteristic frequency of PO_4^{3-}, phosphoryl (P=O) (see Fig. S3). But this peak is absent in HT002, implying that the doped P might not simply exist in the form of PO_4^{3-} but as Ti–O–P. The XPS spectrum of P 2p in Fig. S2(b) consists of a doublet peak of P $2p_{3/2}$ and P $2p_{1/2}$. The binding energy of P $2p_{3/2}$ in HT002 locates at 133.3 eV, indicating the existence of P^{5+}. This value is also different from that of P^{5+} in Na_3PO_4 impregnated TiO_2 which locates at 132.7 eV. As the ionic radii for Ti^{4+} and P^{5+} are not very close (0.67 and 0.38 Å respectively, in an environment of coordination number 6), P^{5+} species are not likely to exist in the bulk with high concentration. Thus, we suggest that doped P may exist on the surface or near surface region in an octahedral environment by replacing part of Ti^{4+}, rather than as PO_4^{3-} in a tetrahedral environment (Table 3).

The O 1s region of HT002 can be fitted by three peaks, which are Ti–O in TiO_2, H–O in hydroxyl groups and C–O in surface contaminants (Fig. S3(c)). Table 3 summarizes the percentage composition of these three kinds of oxygen atoms. With increasing

Table 3
Surface P/Ti molar ratio and relative percentage of O (O–Ti), (O–H) and (O–C) in pure or P-doped titania samples.

Sample	P:Ti	Ti 2p3/2 B.E. (eV)	O 1s (O–Ti) (%)	O 1s (O–H) (%)	O 1s (O–C) (%)
Pure titania	–	458.4	86.6	9.0	4.4
HT001	0.032	458.5	81.8	13.0	5.2
HT002	0.050	458.6	78.9	15.1	6.0
HT004	0.078	458.7	76.5	15.2	6.2
HT008	0.085	458.9	73.5	19.3	7.2
CT002-500	0.053	458.7	80.4	13.9	5.6
CT002-600	0.059	458.7	80.1	14.5	5.4

phosphorous concentration, the percentage of O atom in Ti–O bond decreased, while the content of the other two kinds of O atoms get a steady increase, especially that of the hydroxyl groups. Two reasons account for this. Firstly, the sample with higher P content has larger specific surface area and its surface is more contaminated by carbohydrate which contains oxygen atom in O–H bond or O–C bond. Secondly, as mentioned in above section, P-doping induced additional surface hydroxyl groups. Combining the two factors, the oxygen content in O–H gradually increased as phosphorous concentration gets higher.

In Table 3, it can be seen that HT002, CT002-500 and CT002-600 have nearly the same surface P:Ti atomic ratio, as well as the percentage concentration of the three kinds of O atom. It means that surface properties are mainly decided by the P:Ti stoichiometric ratio, but not the crystallization method. Whether the titania nanoparticles are crystallized by hydrothermal or calcination has little influence on their surface properties.

3.1.5. UV–vis DRS

Fig. 3 shows the optical properties of pure TiO_2 and P-doped samples studied by UV–vis diffuse-reflectance spectroscopy. Pure titania and HT002 have nearly the same absorption edges which locate at 388 and 389 nm, respectively. Further increasing P-doping concentration, a red shift by several nanometers is observed. For HT004 and HT008, the absorption edge moves to 391 and 392 nm, respectively. Calcinated samples have similar absorption behavior to the hydrothermally treated ones (figure not shown for the sake of simplicity). The corresponding band gap energy is summarized in Table S1. It indicates that P-doping decreased the band gap to a small extent, but the red shift of the absorption edge was almost negligible. This phenomenon is in contradiction with previous reports which claimed a blue shift of the band gap caused by phosphate modification due to the quantum size effect [16,20]. Though the actual effect of P-doping on the optical property is still in debate, first principles calculation by the density function theory may shed light on it [28]. Yang et al. calculated the electronic structure of P cation-doped anatase and found that the replacement of P cation (P^{5+}) to Ti^{4+} leads to a slight rise of the valence band, thus causing a tiny narrowing of band gap. This theoretical result is in fully accordance with our experimental conclusion.

The substitution of Ti^{4+} by P^{5+} in the bulk would cause a charge imbalance and has a demand to compensate for this effect, thus diminishing the number of oxygen vacancies. This could be illustrated by the DR spectra of P-doped samples which do not show a sloping baseline or any shoulders in the visible region ($\lambda > 400$ nm),

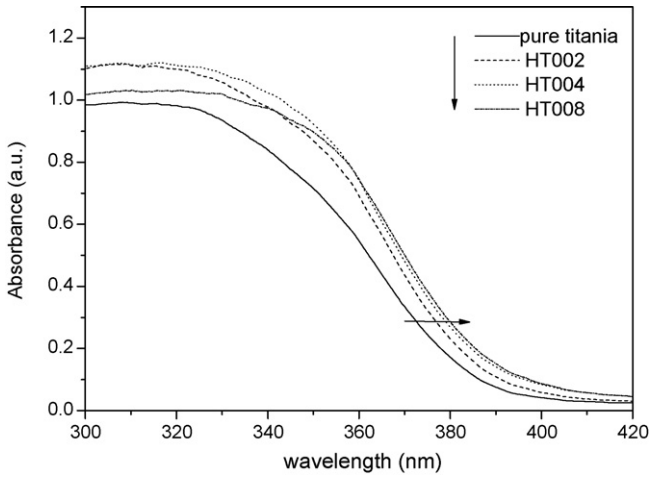

Fig. 3. UV–vis diffuse reflectance spectrum of pure titania, HT002, HT004 and HT008.

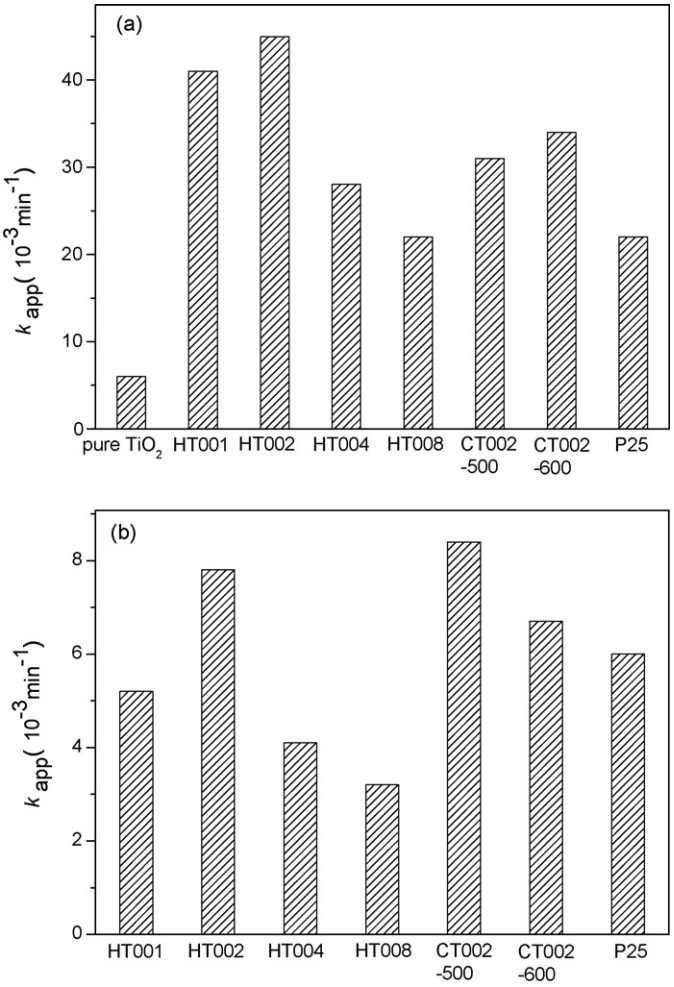

Fig. 4. The degradation rate of MB with pure titania, phosphorous-doped samples and P25 as photocatalyst under (a) UV irradiation and (b) visible light irradiation ($\lambda > 400$ nm).

indicating a minimal oxygen vacancies [29]. Irie et al. and Subbarao et al. reported that oxygen vacancies promote the recombination of holes and electrons [30,31]. Xie found that the substitution of Al^{3+} for Ti^{4+} in TiO_2 would result in the formation of oxygen vacancies in the lattice for the charge balance. The oxygen vacancies present in the TiO_2 lattice acting as effective combination centers of photogenerated electrons and holes were proposed to be responsible for the deactivation [32]. In our case, P^{5+} has a higher valence than Ti^{4+} and would cause an opposite effect compared to Al^{3+}, reducing the numbers of oxygen vacancies and enhancing the photocatalytic activity.

3.2. Photocatalytic property

Photodegradation of MB was employed to evaluate the photocatalytic activities of various catalysts. The initial concentration of MB after achieving adsorption–desorption equilibrium was denoted as c_0. The photodegradation of MB follows roughly the pseudo-first-order reaction and the apparent rate constants were deduced from the linear fitting of $\ln(c_0/c)$ versus reaction time. For comparison, the photocatalytic activity of commercial P25 was also measured under identical conditions.

As can be seen in Fig. 4a, pure titania shows very low photoactivity under UV light, while the best performance was observed with HT002, which is twice that of P25. Higher phosphorous content leads to deterioration of MB degradation rate. The photocatalytic

activity of CT002-600 is also superior to P25, but still 19% lower than that of HT002.

The photoactivity of P-doped samples is also boosted in the visible region at $\lambda > 400$ nm. As illustrated in Fig. 4b, nearly the same MB degradation rate was observed for HT002 (7.8×10^{-3} min^{-1}) and CT002-500 (8.4×10^{-3} min^{-1}), both of which are higher than P25 (6.0×10^{-3} min^{-1}). Other samples with smaller or higher P-doping concentration than HT002 do not show such a decent visible light activity. Pure titania shows almost no activity under visible light irradiation.

P-doping does not greatly extend the absorption edges to the visible region; however, if we scrutinize the UV–vis absorption spectrum between 400 and 420 nm, it is found that the absorption of P-doped samples is slightly higher than that of pure titania in this region. The MB degradation on P-doped titania under >400 nm visible light is likely to be caused by this tiny absorption. We have made a control experiment which was conducted under <420 nm cut-off filter. In this case, MB degradation rate on HT002 was quite low and could be neglected (Fig. S4), proving that P–TiO_2 could mainly utilize the 400–420 nm of visible light.

3.3. Discussion

The above results have shown that, by phosphorous doping, the surface area is significantly enlarged and the changes of surface and bulk properties are great. Additional hydroxyl groups are induced on the surface of nanoparticles and this is known to be a beneficial factor for photocatalytic oxidative reactions. We also propose that the numbers of oxygen vacancies are diminished to compensate for the charge imbalance, which would promote the photocatalytic activity. The overall effect is positive although the crystallization degree is lowered after P-doping. Thus, great improvement of the MB degradation rate was observed even on the sample with phosphorous concentration as low as 1%. Compared to HT002, further increasing the doping level to 8% does not change the surface and bulk properties very much, but would lower the crystallization degree and create recombination centers for electrons and holes, thus worsening its performance.

XPS analysis shows that the surface properties of HT002, CT002-500 and CT002-600 are almost the same. So it is not a decisive factor to illustrate for the different performance between the hydrothermal treated sample and the calcinated ones for the degradation of MB under UV light. Also, these samples do not show much difference in surface area and optical property. Thus, the decent performance of HT002 under UV light can only be accounted by its extremely high crystallization degree against CT002-500 and CT002-600. Hydrothermal method is very suitable for the synthesis of P-doped titania. Samples with high surface area and crystallization degree can be prepared by this way.

4. Conclusion

Well-crystallized P-doped titania nanoparticles were prepared by hydrothermal treatment. The BET surface area of P-doped samples largely exceeds that of pure titania. The charge imbalance caused by P^{5+} substitution is compensated by additional surface hydroxyl groups or the reduction of oxygen vacancies. All these aspects account for the ultrahigh photocatalytic activity of P-doped titania toward the degradation of methylene blue.

In this work, it is shown that hydrothermal method is a promising way to prepare titania nanoparticles with well-crystallinity and high surface area. P-doped titania synthesized by this method exhibits superior photoactivity to the calcined ones and has great potential for the wastewater remediation.

Acknowledgments

The authors are grateful for the financial support of the National Science Foundation of China (20773004), and the Major State Basic Research Development Program (Grant No. 2006CB806102).

Appendix A. Supplementary data

Supplementary data associated with this article can be found, in the online version, at doi:10.1016/j.molcata.2009.07.021.

References

[1] A. Fujishima, K. Honda, Nature 238 (1972) 37–38.
[2] A.L. Linsebigler, G. Lu, J.T. Yates, Chem. Rev. 95 (1995) 735–758.
[3] O. Legrini, E. Oliveros, A.M. Braun, Chem. Rev. 93 (1993) 671–698.
[4] M.R. Hoffmann, S.T. Martin, W. Choi, D.W. Bahnemann, Chem. Rev. 95 (1995) 69–96.
[5] R. Asahi, T. Morikawa, T. Ohwaki, K. Aoki, Y. Taga, Science 293 (2001) 269–271.
[6] S. Somekawa, Y. Kusumoto, M. Ikeda, B. Ahmmad, Y. Horie, Catal. Commun. 9 (2008) 437–440.
[7] Y. Cong, J. Zhang, F. Chen, M. Anpo, J. Phys. Chem. C 111 (2007) 6976–6982.
[8] T. Tachikawa, Y. Takai, S. Tojo, M. Fujitsuka, H. Irie, K. Hashimoto, T. Majima, J. Phys. Chem. B 110 (2006) 13158–13165.
[9] W. Zhao, W. Ma, C. Chen, J. Zhao, Z. Shuai, J. Am. Chem. Soc. 126 (2004) 4782–4783.
[10] S.U.M. Khan, M. Al-Shahry, W.B. Ingler, Science 297 (2002) 2243–2245.
[11] M.S. Wong, S.W. Hsu, K.K. Rao, C.P. Kumar, J. Mol. Catal. A 279 (2008) 20–26.
[12] Y. Xie, X.J. Zhao, J. Mol. Catal. A 285 (2008) 142–149.
[13] T. Umebayashi, T. Yamaki, H. Itoh, K. Asai, Appl. Phys. Lett. 81 (2002) 454–456.
[14] D. Li, H. Haneda, S. Hishita, N. Ohashi, Chem. Mater. 17 (2005) 2588–2595.
[15] H. Luo, T. Takata, Y. Lee, J. Zhao, K. Domen, Y.S. Yan, Chem. Mater. 16 (2004) 846–849.
[16] J.C. Yu, L. Zhang, Z. Zheng, J. Zhao, Chem. Mater. 15 (2003) 2280–2286.
[17] L. Lin, W. Lin, Y.X. Zhu, B.Y. Zhao, Y.C. Xie, Chem. Lett. 34 (2005) 284–285.
[18] Q. Shi, D. Yang, Z. Jiang, J. Li, J. Mol. Catal. B 43 (2006) 44–48.
[19] L. Lin, W. Lin, J.L. Xie, Y.X. Zhu, B.Y. Zhao, Y.C. Xie, Appl. Catal. B 75 (2007) 52–58.
[20] L. Korosi, A. Oszko, G. Galbacs, A. Richardt, V. Zollmer, I. Dekany, Appl. Catal. B 77 (2007) 175–183.
[21] L. Korosi, S. Papp, I. Bertoti, I. Dekany, Chem. Mater. 19 (2007) 4811–4819.
[22] H. Ozaki, N. Fujimoto, S. Iwamoto, M. Inoue, Appl. Catal. B 70 (2007) 431–436.
[23] R. Zheng, L. Lin, J. Xie, Y. Zhu, Y. Xie, J. Phys. Chem. C 112 (2008) 15502–15509.
[24] M.Y.K. Byrappa, Handbook of Hydrothermal Technology, William Andrew Publishing, Inc., New York, 2001.
[25] M. Toyoda, Y. Nanbu, Y. Nakazawa, M. Hirano, M. Inagaki, Appl. Catal. B 49 (2004) 227–232.
[26] C.C. Wang, J.Y. Ying, Chem. Mater. 11 (1999) 3113–3120.
[27] R. Mueller, H.K. Kammler, K. Wegner, S.E. Pratsinis, Langmuir 19 (2002) 160–165.
[28] K. Yang, Y. Dai, B. Huang, J. Phys. Chem. C 111 (2007) 18985–18994.
[29] S.C. Padmanabhan, S.C. Pillai, J. Colreavy, S. Balakrishnan, D.E. McCormack, T.S. Perova, YuriiGun'ko, S.J. Hinder, J.M. Kelly, Chem. Mater. 19 (2007) 4474–4481.
[30] H. Irie, Y. Watanabe, K. Hashimoto, J. Phys. Chem. B 107 (2003) 5483–5486.
[31] S.N. Subbarao, Y.H. Yun, R. Kershaw, K. Dwight, A. Wold, Inorg. Chem. 18 (1979) 488–492.
[32] T.H. Xie, J. Lin, J. Phys. Chem. C 111 (2007) 9968–9974.